Mathematical Model of Cardiovascular and Metabolic Responses to Umbilical Cord Occlusions in Fetal Sheep

Qiming Wang, Nathan G Gold, Martin G Frasch, Huaxiong Huang, Marc Thiriet, Steven Xiaogang Wang

HAL Id: hal-01384265

https://hal.sorbonne-universite.fr/hal-01384265

Submitted on 20 Oct 2016

Mathematical Model of Cardiovascular and Metabolic Responses to Umbilical Cord Occlusions in Fetal Sheep

Qiming Wang†, Nathan Gold†, Martin G. Frasch‡,

Huaxiong Huang†, Marc Thiriet*, and Steven Wang†

†*Department of Mathematics and Statistics,*

York University, Ontario, Canada, M3J 1P3

‡*Department of Obstetrics and Gynecology and Department of Neurosciences,*

Faculty of Medicine at CHU Sainte-Justine Research Center

and Centre de Recherche en Reproduction Animale (CRRA),

Faculty of Veterinary Medicine, Université de Montréal, Quebec, Canada, H3T 1C5

*Sorbonne University, UPMC, Laboratoire Jacques-Louis Lions,

CNRS, UMR 7598, INRIA, EPI REO, 75252, Paris, France

Key points

- A mathematical model is developed for predicting the effects of repetitive intermittent umbilical cord occlusions of variable severity on fetal cardiovascular and metabolic responses.

- Our model is capable of reproducing the salient features observed in the various ovine fetal experimental models such as fetal heart rate (FHR) decelerations, mean arterial blood pressure (MABP) responses, pH, lactate and base deficit (BD) dynamics with worsening mixed respiratory and metabolic academia.

- Our model also shows that the FHR variability, combined with secondary features of FHR (such as overshoots) and MABP decline can serve as indicators of worsening fetal acidemia with increased BD.

Abstract   Fetal acidemia during labour is associated with an increased risk for brain injury and lasting neurological deficits. This is in part due to the repetitive occlusions of the umbilical cord (UCO) induced by the uterine contractions. While fetal heart rate (FHR) monitoring is widely used clinically, it fails to detect fetal acidemia. Hence, new approaches are needed for early detection of fetal acidemia during labour. We built a mathematical

model of the UCO effects on FHR, mean arterial blood pressure (MABP), oxygenation and the metabolism. Mimicking fetal experiments, our *in silico* model reproduces salient features of experimentally observed fetal cardiovascular and metabolic behavior including FHR overshoot, gradual MABP decrease and mixed metabolic and respiratory acidemia during UCO. Combined with statistical analysis, our model provides valuable insight of the labour-like fetal distress and guidance for refining FHR monitoring algorithms to improve detection of fetal acidemia and cardiovascular decompensation.

Abbreviations FHR, Fetal Heart Rate; MABP, Mean Arterial Blood Pressure; UCO, Umbilical Cord Occlusions; BD, Base Deficit, RMSSD, Root Mean Square of the Successive Differences.

I. INTRODUCTION

One of the main issues during childbirth is the possibility of developing severe fetal acidemia (pH < 7.0) caused by umbilical cord occlusions (UCO) due to repetitive uterine contractions. The resulting increased risk of schemic brain injury can be associated with acidemia [1]. The sudden compression of the umbilical cord leads to fetal hypertension and fetal heart rate (FHR) decelerations, which are mediated through chemoreflex and sympathetic stimulation [2–4]. Fetal oxygen delivery via umbilical cord is interrupted and leads to hypoxemia and acute cerebral hypoxia [5–10]. In addition, FHR reduction and oxygen deficiency also activate sympathetic and parasympathetic brainstem centers resulting in changes of afferent and threshold efferent firing rates [11, 12]. These activities, in turn, via efferent signaling, regulate FHR and systemic arterial blood pressure. Furthermore, prolonged cord compression and/or repeated cord compressions may cause accumulation of metabolites, such as CO_2 and lactate, in the fetus, which contributes to acidemia [4, 13], as well as prolonged cerebral hypoperfusion [14]. A comprehensive discussion on the dynamic changes of the fetal circulation and blood flow distribution during hypoxia and asphyxia due to different experimental disturbances can be found in a review paper [15].

Beyond the physiological understanding of the general process, a clinically relevant question is how to monitor and predict the levels of fetal acidemia based on the available clinical data so that the fetal brain can be protected by medical intervention. Since direct continuous measurements of acidemia from fetal blood are not possible clinically and measurements can

only be done intermittently in an animal model, attempt has been made to use statistical approaches to make prediction of acidemia based on FHR [16]. However, current FHR-based clinical algorithms do not provide an accurate prediction of acidemia [17]. This is because there is no *a priori* knowledge of which FHR properties reflect acidemia best. Therefore, a mechanistic modeling approach that can identify FHR properties related to acidemia will provide valuable insights that are useful for developing more effective diagnostic tools.

Mathematical modeling and simulation are useful alternatives to experiments, especially when they are too difficult or too expensive. One of the advantages of mathematical models is that they allow us to conduct parametric studies easily. The physical quantities can be easily tracked. A popular mathematical model in describing the cardiovascular system coupled with the central nervous system has been proposed by Ursino [18], followed by many related studies that can reproduce and predict the cardiovascular responses in various systems successfully [19–23]. The drawback is that usually the biological system has a large number of parameters, some of which are difficult or impossible to measure. This makes analysis difficult and can easily introduce uncertainties and errors in the model. A similar cardiovascular mathematical model was used to explore physiological mechanisms in postural change and related physiology problems [24–26]. The common ground of those models shared is the electric circuit analog, but in the meantime, Olufsen's group also performed mathematical analysis and sensitivity analysis [26] to better understand the model dynamics and the impact of the parameters on outputs. A recent review on various models can be found in [27].

The metabolic dynamics formulated using a deterministic approach, is based on the cardiovascular model by Olufsen's group and a similar (local) sensitivity analysis. A regulation model is incorporated to provide cardiovascular feedback with respect to the arterial pressure and substrate (oxygen, lactate, glucose $\cdots$) concentrations via central neural system, following the works in [18, 21, 23, 28]. Details are revealed in section II. Furthermore, current modeling includes biochemical processes with proper substrate transfer between blood and organs is incorporated. As indicated by the experiments [13, 29], metabolic dynamics is closely related to the development of acidemia in fetal sheep and accumulation of wastes, such as CO_2 and lactate, contributes to the decline in pH. A mathematical model can continuously display both in time and space the evolution of implicated molecular concentrations, unlike measurements.

3

The present mathematical model consists of three elements: a lumped parameter model for the cardiovascular circuit coupled with nervous regulation and reciprocal perfusion–metabolism influences. This model is used to investigate the effect of UCOs on FHR, MABP pattern and acidemia development. Our model reproduces some of the patterns observed in animal experiments such as FHR overshoot, deceleration, MABP and pH decline, lactate and CO_2 increase. More importantly, we have confirmed correlation between RMSSD, a statistical measure of FHR variability and critical levels of lactate and pH. On the other hand, we have also shown that one has to be careful when applying RMSSD as a predictive index. In particular, a variable window size should be used to compute RMSSD when the occlusion duration varies instead of blindly applying standard signal processing techniques.

The rest of the paper is organized as follows. The model equations are given in section II for different components. In section III, model calibration is discussed and a sensitivity analysis is carried out to identify the most sensitive parameters in the mathematical model. Numerical results motivated by different fetal experiments are presented in cardiovascular responses in section III B and metabolic dynamics in section III C. Statistical analysis based on contingency table and RMSSD are discussed in section III D. Finally a summary and conclusion are given in section IV.

II.   MATHEMATICAL FORMULATION

A.   Cardiovascular system

Our model includes both maternal and fetal circulations. Similar to previous studies [24, 28], we use the electrical circuit analogs, where pressure $p(t)$ is analogous to voltage, volumetric flow rate $q(t)$ to the current, and compliance C_i to capacitance. In addition, the resistance R accounts for the viscous pressure drop in each element of the circuit. A schematics of the model with individual components is given in Fig. 1. We model the heart (both in the maternal and fetal circulation) as an effective left ventricle [24], which has two ideal valves on two sides. Two compartments are used to model the branching flow before and after the ventricle, where p_a and p_v are computed [24]. Our model hearts are effective pumps that produce the desirable cardiovascular outputs to maintain both maternal and fetal blood circulations. The fetal systemic circulation is modeled as one compartment with subscript
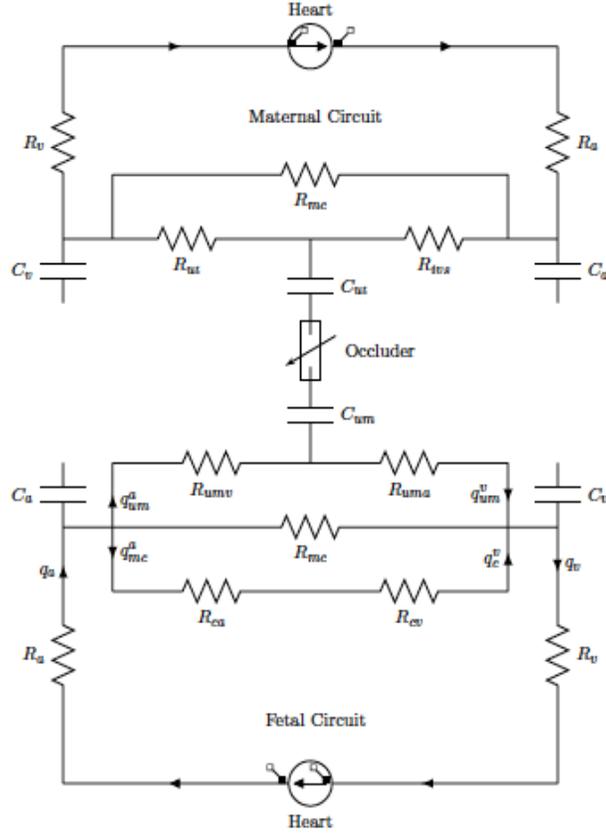
FIG. 1. **Illustration of model setup.** Our model includes two circulatory networks: maternal circulation (top) and fetal (bottom) circulations. Resistors R and compliances C are indicated, arrows giving blood flow direction, similar to [28]. In this mathematical domain sketch, 'a' stands for artery, 'v' for vein, 'um' for umbilical cord, 'mc' for systemic part, 'c' for cerebral part, 'ut' for uterine and 'ivs' for intervillous space.

'mc' (Fig. 1). While the remaining fetal circulation is considered as one compartment, the umbilical cord and cerebral circulation are modeled separately with arteries and veins [28]. The maternal circulation system is coupled with the fetal circulation system through partial oxygen pressure in intervillous space of the placental connected to the umbilical cord. We adopt an oxygen transport model [30] and the oxygen distribution in the circulation systems is given by the conservation of mass [28] including convection, diffusion and reaction (metabolic uptake and consumption) in the circuit. The blood pressure and oxygen content are coupled through a regulatory model on heart rate by the vagal–sympathetic control [18, 28].

5

The basic equations predicting blood pressure and flow can be obtained by computing the volume V and its change for each compartment, $V = Cp$, where C is the compliance, which plays the role of capacitance and p is the pressure for the corresponding compartment. The change of volume in each compartment is then given by

$$\frac{dV}{dt} = q_{in} - q_{out}. \tag{1}$$

Analogy to the Ohm's law provides a linear relation between pressure p and flow rates q

$$q_i = \frac{p_{in} - p_{out}}{R_i}, \tag{2}$$

where the subscript i stands for a (artery), v (vein), um (umbilical), c (cerebral; Fig.1). In this study only the resistance in system is modelled while inertia is neglected [24] . With compliances kept as constants, the equations for pressure change are given by

$$C_i \frac{dp_i}{dt} = q_{in} - q_{out}. \tag{3}$$

The fetal heart is modeled similarly as the left ventricle used in the study [24] (a combined ventricle) where the details in pulmonary circulation and the ductus arteriosus are ignored. The rate of volume change [24], is given by

$$\frac{dV_h}{dt} = s_{mv}q_{mv} - s_{av}q_{av}, \tag{4}$$

where s_{mv} and s_{av} are the indicator functions for valves with zero and one for a closed and open valve, respectively. Conservation of volume V requires that $dV_{total}/dt = 0$, where V_{total} is the total volume of all compartments [24]. To model the branching before and after the ventricle, flow rate satisfies the law of mass conservation [24, 25, 28], given by

$$q_{av} = q_c^a + q_{mc} + q_{um}^a, \tag{5}$$

$$q_{mv} = q_c^v + q_{mc} + q_{um}^v. \tag{6}$$

The pressure-volume relationship is given by [24]

$$p_h = a(V_h - b)^2 + (c(t)V_h - d)g(t), \tag{7}$$

where V_h, p_h, and $c(t)$ are the heart volume, pressure, and contractility, respectively. Here $g(t) = f(t)/f(t_p)$ is an activation function that controls periodic oscillation. In maternal

6

circulation, $c(t) = c_m$ is assumed to be a constant, while in fetal circulation $c(t) = c_f(t)$ is regulated by β sympathetic activity (see 35 below) and $f(t)$ is given by [24],

$$f(t) = \begin{cases} p_p(H)\frac{t^n(\beta(H)-t)^m}{n^n m^m((\beta(H)-\alpha)/(m+n))^{m+n}}, & 0 \le t \le \beta_h(H), \\ 0, & \beta_h(H) < t \le T \end{cases}$$

where H is the heart rate controlled by the nervous system (Section II D), n and m characterize the contraction and relaxation phases, t_p and p_p are the peak time and peak value of the activation, and $\beta_h(H)$ is the time when the valve is closed and flow stops. According to [24], the expressions for t_p, p_p and $\beta_h(H)$ are given by

$$t_p = t_{min} + \frac{\theta^\nu}{H^\nu + \theta^\nu}(t_{max} - t_{min}), \tag{8}$$

$$p_p = p_{min} + \frac{H^\eta}{H^\eta + \phi^\eta}(p_{max} - p_{min}), \tag{9}$$

$$\beta_h(H) = \frac{n+m}{n}t_p(H) \tag{10}$$

where ν and η are parameters that control the steepness of the sigmoidal change. Blood is pumped out from heart into arterial system and flows through each individual compartment such as the umbilical cord, cerebral and systemic compartment in fetal circulation system, and returns to the heart via vein (Fig.1).

B. Metabolic model

The model for oxygen distribution is based on mass conservation [28, 30]. Oxygen concentration $[O_2]$ in each compartment is given by the following equations

$$\frac{d([O_2]_{ivs}V_{ivs})}{dt} = q_{ivs}([O_2]_{in}^m - [O_2]_{ivs}) - S_{O_2,d}, \tag{11}$$

$$\frac{d([O_2]_{um}V_{um})}{dt} = q_{um}^a([O_2]_{in} - [O_2]_{um}) + S_{O_2,d}, \tag{12}$$

$$\frac{d([O_2]_c V_c)}{dt} = q_c^a([O_2]_{in} - [O_2]_c) - O_{met,c}, \tag{13}$$

$$\frac{d([O_2]_{mc}V_{mc})}{dt} = q_{mc}([O_2]_{in} - [O_2]_{mc}) - O_{met,mc}, \tag{14}$$

where the subscript ivs stands for the intervilious space. V_i is the blood volume in compartment i, q_i is the flow through the compartment. The feeding oxygen concentration in fetus is given by

$$[O_2]_{in} = \frac{[O_2]_{um}q_{um}^a + [O_2]_{mc}q_{mc} + [O_2]_c q_c^a}{q_{av}}, \tag{15}$$

7

while $[O_2]_{in}^m = 0.2$ is fixed in maternal part [30]. $S_{O_2,d}$ and $O_{met,i}$ account for diffusion and metabolic uptake, respectively [28, 30]. The oxygen diffusion in the placenta is determined by the oxygen partial pressure difference between the intervillous space and the umbilical cord (or umbilical microcirculation),

$$S_{O_2,d} = D(P_{O_2^{ivs}} - P_{O_2^{um}}) \tag{16}$$

with P_{O_2} being the partial oxygen pressure and D is the mass transfer coefficient. The oxygen concentration is related to the oxygen partial pressure by the following relation (subscript omitted)

$$[O_2] = \frac{\alpha Hb S(P_{O_2})}{100} + \beta P_{O_2}, \tag{17}$$

where α represents the maximum binding capacity of hemoglobin, Hb the hemoglobin concentration and β the content of dissolved oxygen. In addition, S in (17) is given by

$$S(P_{O_2}) = \frac{100}{1 + c_1(P_{O_2}{}^3 + c_2 P_{O_2})^{-1}}. \tag{18}$$

The metabolic uptake in equations (13, 14) is a constant when the oxygen supply is sufficient. When oxygen concentration drops below a threshold concentration, $[O_2]_{th}$, it is assumed to be a linear function of the oxygen concentration. Combining the two, we have

$$O_{met} = \begin{cases} O_{met,0}, & [O_2] \geq [O_2]_{th}, \\ O_{met,0} + K([O_2] - [O_2]_{th}), & [O_2] < [O_2]_{th} \end{cases}$$

for all fetal compartments [28]. In maternal circulation, we assume that oxygen supply is sufficient [28, 30].

As an indicator for asphyxia (due to prolonged UCO typically), we model CO_2 distribution, using the law of mass conservation equation for CO_2 in each fetal compartment as following

$$\frac{d([CO_2]_{um} V_{um})}{dt} = q_{um}^a([CO_2]_{in} - [CO_2]_{um}) + D_{CO_2}(P_{CO_2}{}^{ivs} - P_{CO_2}{}^{um}), \tag{19}$$

$$\frac{d([CO_2]_c V_c)}{dt} = q_c^a([CO_2]_{in} - [CO_2]_c) + M_c, \tag{20}$$

$$\frac{d([CO_2]_{mc} V_{mc})}{dt} = q_{mc}([CO_2]_{in} - [CO_2]_{mc}) + M_{mc} + M_{pH}, \tag{21}$$

where $[CO_2]_{in}$ is given by

$$[CO_2]_{in} = \frac{[CO_2]_{um} q_{um}^a + [CO_2]_{mc} q_{mc} + [CO_2]_c q_c^a}{q_{av}}. \tag{22}$$

8

D_{CO_2} is the diffusion coefficient, P_{CO_2} the partial pressure of carbon dioxide, M_i the production rate of $[CO_2]_i$ and M_{pH} is given by

$$M_{pH} = 0.1 \frac{([H^+] - 40)^2}{1 + ([H^+] - 40)^2}. \tag{23}$$

We assume that CO_2 is cleared in the placenta and $P_{CO_2}{}^{ivs} = 40$ mmHg is fixed. In addition, we assume that the production of carbon dioxide is related to the metabolic rate of oxygen and $M_{CO2} = K O_{met}$ [31] with a constant K (taken to be 0.2 in this study). The partial pressure of carbon dioxide relates to the concentration linearly as [32]

$$[CO_2] = K_{CO_2} P_{CO_2} + k_{CO_2}, \tag{24}$$

where K_{CO_2} and k_{CO_2} are scaling constants.

To assess the acidity level [13, 17, 33], lactate and pH values that are usually measured in fetal animal experiments, are include in our model (Fig. 2). Following [34, 35], we consider
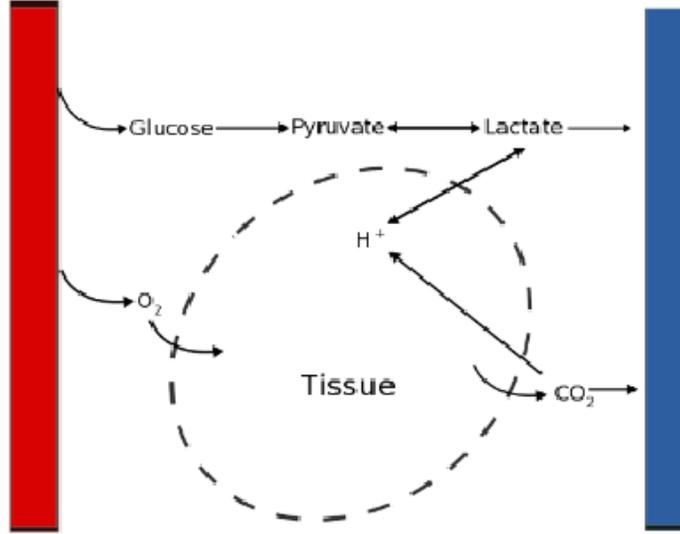
FIG. 2. Illustration of the simplified metabolic process in certain compartment in the model. Left (right) column stands for artery (vein).

pyruvate, glucose and lactate related metabolic pathways in the fetal body or systemic compartment, in particular, anaerobic glycolysis, pyruvate reduction, glycoeogenesis, glycogen synthesis and breakdown, lactate oxidation, lactate buffering. The equations for glucose (GL), lactate (LA) and pyruvate (PY), from literature [35], which is solving a coupling

between cardiovascular and metabolism for excises, are

$$V\frac{d[\text{GL}]}{dt} = q\left(\text{GL}_{in} - [\text{GL}]\right) + m\phi_{GYb}\frac{PS}{PS + k_{GYb}}[GY]$$

$$- \phi_{GLb}\frac{PS}{PS + k_{GLb}^{PS}}\frac{[\text{GL}]}{RS/k_{GLb}^{RS} + 1} - \phi_{GYs}\frac{[\text{GL}]}{PS/k_{GYs} + 1} \qquad (25)$$

$$V\frac{d[\text{PY}]}{dt} = q\left(\text{PY}_{in} - [\text{PY}]\right) + 2\phi_{GLb}\frac{PS}{PS + k_{GLb}^{PS}}\frac{[\text{GL}]}{RS/k_{GLb}^{RS} + 1}$$

$$- \phi_{PYr}\frac{RS}{RS/k_{PYr} + 1}[PY] - \phi_{PYo}\frac{RS}{RS/k_{PYo} + 1}[PY]$$

$$+ \phi_{LA}\frac{1}{RS/k_{LAo} + 1}[\text{LA}] \qquad (26)$$

$$V\frac{d[\text{LA}]}{dt} = q\left(\text{LA}_{in} - [\text{LA}]\right) + \phi_{PYr}\frac{RS}{RS/k_{PYr} + 1}[PY] - \phi_{LA}\frac{1}{RS/k_{LAo} + 1}[\text{LA}] \qquad (27)$$

where the first term on the right hand side of the equations models convective exchange, $[*]_{in}$ is the arterial concentration (Eq. (15)), $PS = [ADP]/[ATP]$ and $RS = [NADH]/[NAD]$, which are picked as constants in [34] as 0.13 and 0.11 respectively, GY is Glycogen whose concentration is much larger than the rest (table 2 in [34]) and hence is treated as a constant in current model, $\phi_{[*]}$ is the reaction rate accordingly and $k_{[*]}$ are constants. In addition, the subscripts are short names for different stoichiometry $GYb(\text{GY} \to \text{mGL})$, $GYs(\text{mGL} \to \text{GY})$, $GLb(\text{GL} \to 2\text{PY})$, $LAo(\text{LA} \to \text{PY})$, $PYr(\text{PY} \to \text{LA})$.

A close inspection reveals that the kinetic coefficients in front of substrates are effectively (unknown) constants and we tune those to fit the experimental measurements. Using simplifying notations, we obtain

$$\frac{dV[\text{GL}]}{dt} = q\left(\text{GL}_{in} - [\text{GL}]\right) + K_1 - K_2[\text{GL}], \qquad (28)$$

$$\frac{dV[\text{PY}]}{dt} = q\left(\text{PY}_{in} - [\text{PY}]\right) + K_3[\text{GL}] - K_4[\text{PY}] + K_5[\text{LA}], \qquad (29)$$

$$\frac{dV[\text{LA}]}{dt} = q\left(\text{LA}_{in} - [\text{LA}]\right) + K_6[\text{PY}] - K_5[\text{LA}], \qquad (30)$$

where K_i are constants. Constant concentrations for GL, PY, LA are imposed in cerebral and umbilical cord compartments (Table II). This needs to be modified when asphyxia is fully developed [14], which is beyond of the scope of current paper.

The effect of pH is not included in lactate equation (30), which is modified by adding the production due to deprotonation of lactic acid,

$$\frac{dV[\text{LA}]}{dt} = q\left(\text{LA}_{in} - [\text{LA}]\right) + K_6[\text{PY}] - K_5[\text{LA}] + K_{10}[\text{H}^+]. \qquad (31)$$

In addition, we add an equation for $[H^+]$ which takes into account two sources of acidity: lactate dehydrogenase and CO_2 accumulation, since under umbilical cord occlusion, experimental reports show significant waste accumulation (especially CO_2). We use the following equation [36]

$$\frac{dV[H^+]}{dt} = q\left(H_{in} - [H^+]\right) + K_7[LA] + K_8[CO_2] - K_9, \tag{32}$$

where K_7 and K_8 are coefficients for $[H^+]$ accumulation due to increased level of lactate and CO_2; K_9 accounts for the ATP consumption among other effects, which is assumed to be an effective constant that helps to restore normal $[H^+]$ level.

C. Effectors

Following [18, 23], there are a few effectors in the model. For autoregulation in fetal brain, we use the following equation [23],

$$\frac{dR_{cmc}}{dt} = \frac{R^*_{cmc} - R_{cmc}}{\tau_{Rcmc}} \tag{33}$$

where

$$R^*_{cmc} = \frac{R_{cmc,min} + R_{cmc,max} e^{\left(\frac{[O_2]_a - [O_2]_{a,n}}{k_{cmc}}\right)}}{1 + e^{\left(\frac{[O_2] - [O_2]_{a,n}}{k_{cmc}}\right)}} \tag{34}$$

Once the oxygen is low, the reduced resistance will allow more flow to the brain. This acts in opposite direction as the one in systemic circulation (Eq. 37).

The fetal heart contractility $c_f(t)$ in Eq. (7) is regulated by sympathetic nervous control that targets mainly β-adrenergic receptors with a firing rate f_{sh} (Section II D).

$$\triangle c = G_c \ln\left(\frac{f_{sh} - f_{es,min} + f_{s1}}{f_{s1}}\right) \tag{35}$$

which is set to zero if $f_{sh} < f_{es,min}$.

The compliance C_v and resistance R_{mc} [23] are regulated by sympathetic nervous system that targets mainly α-adrenergic receptors with a firing rate f_{sp},

$$\triangle C_v = G_v \ln\left(\frac{f_{sp} - f_{es,min} + f_{s1}}{f_{s1}}\right), \tag{36}$$

$$\triangle R_{mc} = \frac{R_{mc,min} + R_{mc,max} e^{\left(\frac{f_{sp} - f_{sp,n}}{k_{rmc}}\right)}}{1 + e^{\left(\frac{f_{sp} - f_{sp,n}}{k_{rmc}}\right)}}. \tag{37}$$

11

D. Afferent/efferent pathways

Changes in blood and oxygen partial pressures trigger nervous responses via baro- and chemoreceptors. Their effects on heart rate have been described [18, 21, 23], modified in the present work, and incorporated in the model. In particular, the period of heart pumping motion T, is given by $T = T_0 + \triangle T_s + \triangle T_v$, where $T_0 = \tau_0 + T_{s0} + T_{v0}$ with τ_0 an offset term, $T_{s,v0}$ the baseline values of sympathetic/vagal contribution and $\triangle T_v, \triangle T_s$ are determined by

$$\frac{d\triangle T_v(t)}{dt} = \frac{1}{\tau_{T,v}} \left(-\triangle T_v(t) + G_{T,v} f_v(t - D_{T,v}) - T_{v0} \right), \tag{38}$$

$$\frac{d\triangle T_s(t)}{dt} = \frac{1}{\tau_{T,s}} \left(-\triangle T_s(t) + \bar{G}_{T,s} f_s(t - D_{T,s}) + G'_{T,s} \left(f_s - f_{s0} \right) \right). \tag{39}$$

Here $\tau_{T,v}$ and $\tau_{T,s}$ are the respective time constant, $G_{T,v}$ and $\bar{G}_{T,s}, G'_{T,s}$ the gains, $D_{T,v}$ and $D_{T,s}$ the delay of the vagal and sympathetic responses. In the results presented in this paper, they are set to zero. At equilibrium state, the second and third terms in the right hand side of Eqs. 38 and 39 vanish, which leads to $\triangle T_v \to 0$ and $\triangle T_s \to 0$, so that the baseline period is recovered at $T = T_0$. Finally, f_v and f_s are given by

$$f_v = W_{b,v} \frac{f_{ev,min} + f_{ev,max} e^{(f_{ab}-f_{ab,n})/k_{ev}}}{1 + e^{(f_{ab}-f_{ab,n})/k_{ev}}} + W_{c,v} f_{ac} + f_{vh}, \tag{40}$$

$$f_s = \ln \left(\frac{f_{sh} - f_{es,min} + f_{s1}}{f_{s1}} \right), \tag{41}$$

with

$$f_{vh} = \frac{f_{vh,min} + f_{vh,max} e^{(P_{O_{2c}}-P_{O_{2c,0}})/k_{vh}}}{1 + e^{(P_{O_{2c}}-P_{O_{2c,0}})/k_{vh}}} - f_{v,o}, \tag{42}$$

$$f_{sh/sp} = f_{es,\infty} + (f_{es,0} - f_{es,\infty}) e^{k_{es}\left(-W_{b,sh/sp} f_{ab} + W_{c,sh/sp} f_{ac} - f_{sh/sp,o} \right)}, \tag{43}$$

where f_{ab} and f_{ac} are the afferent baro- and chemoreceptor firing rates, respectively, and $f_{sh/sp,o}$ is the hypoxia offset that creats a threshold for sympathetic response. In addition, $f_s = 0$ when $f_{sh/sp} < f_{es,min}$, and $f_s = f_{es,max}$ when $f_{sh/sp}$ exceeds a threshold value $f_{es,max}$. Furthermore, the baro- and chemoreceptors afferent firing rates f_{ab} and f_{ac} are governed by the following first order ODE [23]

$$\frac{df_{ab}}{dt} = \frac{f_{ab}^* - f_{ab}}{\tau_{ab}}, \quad \frac{df_{ac}}{dt} = \frac{f_{ac}^* - f_{ac}}{\tau_{ac}}, \quad \frac{d\bar{p}}{dt} = \frac{p_a - \bar{p}_a}{N_p} \tag{44}$$

where according to [37]

$$f_{ab}^* = \frac{f_{ab,min} + f_{ab,max}e^{\frac{\bar{p}-p_n}{\tau_{kab}}}}{1 + e^{\frac{\bar{p}-p_n}{\tau_{kab}}}}, \tag{45}$$

$$f_{ac}^* = \frac{f_{ac,max} + f_{ac,min}e^{\frac{P_{O_{2a}}-P_{O_{2n}}}{\tau_{kac}}}}{1 + e^{\frac{P_{O_{2a}}-P_{O_{2n}}}{\tau_{kac}}}} \left(\bar{K} \ln \left(\frac{P_{CO_2}^{mc}}{P_{CO_2,n}^{mc}} \right) + 1 \right), \tag{46}$$

$$\bar{p}_a = \frac{1}{N_p} \int_0^t p_a(s)e^{-\psi(t-s)}ds, \tag{47}$$

where $\bar{p}_a$ is the mean arterial blood pressure. The formula used in [23] is recovered when $P_{CO_2}^{mc}$ is in the normal range and f_{ac} rises when $P_{CO_2}^{mc}$ increases. Unless otherwise stated, $\bar{K} = 1$.

The normalization factor N_p is introduced to ensure that the correct mean arterial blood pressure is calculated [24],

$$N_p = \int_0^t e^{-\psi(t-s)}ds = \frac{1 - e^{-\psi t}}{\psi}. \tag{48}$$

The offset value $f_{sh/sp,o}$ in Eq. (43) is determined by

$$\frac{df_{sh/sp,o}}{dt} = \frac{f_{sh/sp,o}^* - f_{sh/sp,o}}{\tau_{isc}} \tag{49}$$

where

$$f_{sh/sp,o}^* = \frac{f_{sh/sp,min} + f_{sh/sp,max}e^{\left(\frac{P_{O_{2a}}-P_{O_{2a,n}}}{k_{isc,sh}}\right)}}{1 + e^{\left(\frac{P_{O_{2a}}-P_{O_{2a,n}}}{k_{isc,sh}}\right)}}. \tag{50}$$

Due to hypoxemia in fetal circulation, the vagal firing rate increases, hence decreasing FHR. The sympathetic response has the opposite effects [11, 38].

To take into account of the apparent mutual inhibition of sympathetic and vagal nerves, we model the sympathetic gain $\bar{G}_{T,s}$ as a sigmoidal function of vagal firing rate f_v,

$$\bar{G}_{T,s} = \frac{\delta G_T e^{\frac{f_v - f_{v_n}}{\tau_{gs}}}}{1 + e^{\frac{f_v - f_{v_n}}{\tau_{gs}}}}, \tag{51}$$

which shows the sympathetic gain tends to the minimal value as the vagal firing rate increases due to the inhibition effect as mentioned. Similarly, we introduce the following for the vagal gain $G_{T,v}$

$$G_{T,v} = \frac{G_{Tv,max} + G_{Tv,min}e^{-\frac{f_{sh}-f_{sh_n}}{\tau_{gv}}}}{1 + e^{-\frac{f_{sh}-f_{sh_n}}{\tau_{gv}}}}, \tag{52}$$

It was pointed out [39–41] that the gains may depend on pressure and other dynamic variables. For simplicity, they are chosen as constants in current model. Meanwhile, we assume that the sympathetic and vagal activity in system are mutually inhibitory and mediated via the chemoreceptors and baroreceptors (see (51) and (52)), which is consistent with the physiological explanations [9].

In summary, the above set of equations form a coupled system. Due to the nonlinear nature of the equations, they are solved numerically using Matlab solver `ode15s` and subroutines `sens_sys` and `sens_ind`, which are given in [42], for sensitivity analysis.

III. RESULTS AND DISCUSSION

Two control parameters are used to measure UCO severity: 1) the ratio between the occlusion and the recovery durations and 2) the occlusion degree (partial or complete). As we show below, the effects of these parameters on FHR are significant.

A. Model calibration: baseline values and sensitivity analysis

As in many cardiovascular models [18, 24, 28], the parameter space is large. Most of the parameter values are obtained from the literature and the remaining ones are calibrated by comparing our model outputs with available experiments. For example, $G_{Tv} \sim 0.04$ is taken instead of 0.09 used for the adult model [18, 28] to reflect the fact that the vagal control in fetus is not as mature. $G'_{T,s}, \delta G_T$ are tuned to achieve a reasonable reduction in FHR for fetus. The values of adjusted parameters are given in Tables I and II.

1. Baseline case

Several important and clinically relevant quantities are listed in Table III, which is the baseline case used for our model calibration. The predicted values from our model are consistent with experimental data. At the onset of a complete UCO, the flow rate in umbilical cord $q_{um}^{a,v} = 0$ and O_2 exchange $S_{O_2,d} = 0$ in the corresponding transport equations (Section II). The flow is stopped in the umbilical cord compartment and the O_2 and CO_2 cannot be delivered continuously between placental and fetal circulations. Mild and moderate UCOs

14

represent partial occlusions, where the passed flow is set to be 50% and 25% of the normal case respectively [33]. The severe case refers to as the complete occlusion regarding the degree.

From the experimental point of view, FHR and MABP are two important quantities often used in modeling and monitoring fetal acidemia with FHR being the single quantity available clinically. One important feature of FHR in experiments with repetitive UCOs is its significant drop during occlusions. In our model it is assumed that the sympathetic and vagal activities are mutually inhibitory and mediated via baro- and chemoreceptors (Eqs. 51 and 52) [9]. FHR does not change markedly when these mechanisms are blocked [23].

FHR overshoot and MABP decline are determined by systemic vascular resistance, myocardial contractility, and venous compliance under the central nervous control as proposed in the literature [23]. We tune the parameters G_c and G_v in Eqs. (35) and (36) for the myocardial contractility and venous compliance, respectively, to achieve FHR overshoot and MABP decline comparable to experimental data. In most cases, sufficient control is achieved with $G_v = 0$, namely, the venous compliance is chosen as a constant [24]. However, for 1:5 UCO, a nonzero G_v is used to reproduce experimental data [3, 29].

2. Sensitivity analysis

We carry out a local sensitivity analysis on model parameters according to [26], using Matlab subroutines, `sens_sys` and `sens_ind` [42].

Suppose the system of equations can be written as

$$\frac{d\boldsymbol{X}}{dt} = F(\boldsymbol{X}, t, \boldsymbol{p}),$$ (53)

where $\boldsymbol{X}$ denotes the state variables, and $\boldsymbol{p} = [p_1, p_2, \cdots p_n]$ stands for the parameters. Then the relative sensitivity matrix is defined as

$$S_{ij}(t, \boldsymbol{p})|_{\boldsymbol{p}=\boldsymbol{p}_0} = \frac{\partial X_i(t, p)}{\partial p_j} \frac{p_j}{X_i(t, p)}|_{\boldsymbol{p}=\boldsymbol{p}_0}, \quad p_j, X_i \neq 0.$$ (54)

We compute a maximum relative sensitivity

$$\boldsymbol{S}_j = \max_i \left(\max_k S_{ij}(t, p) \right)|_{\boldsymbol{p}=\boldsymbol{p}_0}.$$ (55)

We conduct simulations over a period of 500 seconds during which data were recorded. A ranking of parameter sensitivity (Fig. 3) and associated histogram (Fig. 4) illustrate

15

the distribution of most to least sensitive parameters. Some parameters appearing in the regulation model are most sensitive. Many kinetic coefficients appear to be less sensitive [45]. We listed top 10 most sensitive parameters in table IV with their effects.

Our simulation approach differs from that of [26], in which high quality data were available. In that case, an optimization procedure is used to fit model output to experimental data. The sensitivity analysis further helps to reduce the computational cost as optimizing the most sensitive parameters suffices to obtain robust results. Unfortunately, we do not have high quality experimental data as in [24] at this stage. Our sensitivity analysis can only point out most important controlling parameters that can guide potentially future experiments.

B. Cardiovascular dynamics: FHR and MABP hehavior

We studied the one minute occlusion scenario, a clinically relevant case. The recovery time for one minute complete occlusion, that is, the UCO frequency, influences the system behavior significantly. Based on our *in silico* experiments, for 1:2.5 UCO, FHR overshoot appears after about two and half hours and acidosis develops, as demonstrated *in vivo* [3, 4, 29]. In contrast, 1:5 UCO scenario does not show any significant FHR overshoots and acidosis, as shown in the literature [29]. The numerical results displayed in Fig. 5, show the typical time variations of FHR and MABP at the early and late stages of occlusion, respectively. For 1:2.5 UCO, FHR deceleration appears once the occlusion starts. The pronounced FHR overshoot occurs only after a delay of approximately 3 hours, in agreement with experiments [29]. This is accompanied by an eventual decline in MABP after approximately 2 hours. At the early stage of the occlusions, MABP rises as soon as the occlusion starts [4, 17]. The inset in the bottom panel of Fig. 5 (for 1:5 UCO) shows that MABP rises during each occlusion period, even after numerous repetitive occlusions, as expected, but this initial rise tends to disappear in 1:2.5 UCO (left bottom panel). This is again in agreement with experiments [43], hypotension being expected when pH drops below 7.2. The difference in 1:5 and 1:2.5 UCOs indicates that with a sufficient time for recovery, the regulation is able to maintain the blood pressure level and avoid instability. The detailed mechanism is still unknown and in the real situation, the regulatory functions represented by Eqs. (35) and (36) may depend on time-dependent or memory-related factors. Overall, the
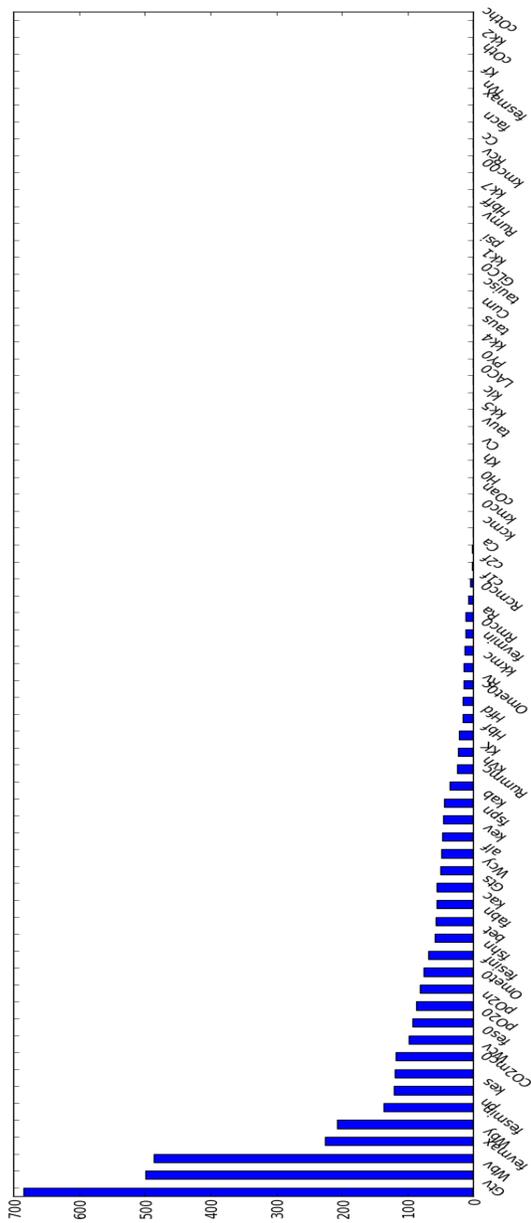
FIG. 3. Results of sensitivity for 70 parameters used in the model. The vertical axis is calculated based on Eq. (55).
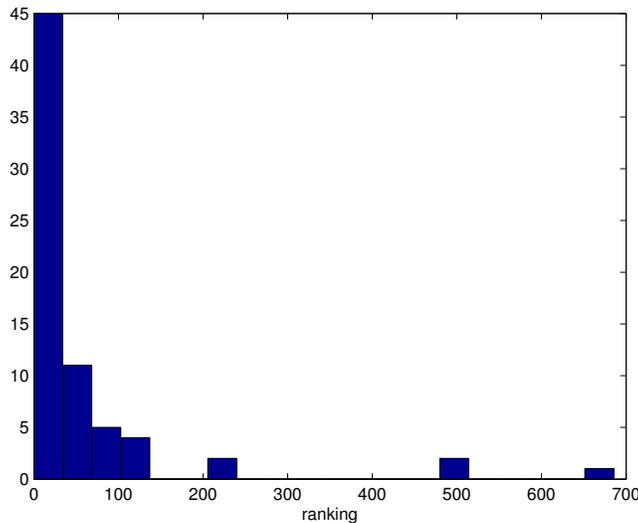
FIG. 4. Histogram of ranked parameters showing the distribution from most to least sensitive parameters.

results in Fig. 5 demonstrate a reasonable agreement between experimental and numerical data. We will compute the correlation of FHR, MABP, and acidosis in Section III D, as well as the output of the metabolic model.

In addition, intermediate rise occurs typically in FHR and MABP in each occlusion for 1:2.5 UCO, when the FHR overshoot is pronounced. Similar intermediate rise was reported in [3], where in the UCO 1:2.5 group, FHR initially recovers after the occlusion but rapidly falls again before returning to the baseline value eventually. In our case, the trend is similar but it appears earlier than experiments, with a relatively larger magnitude. We suspect that it is caused by some system delay factor. Eqs. 38 and 39 contain delay variables D_{T_v} and D_{T_s}. These are set to zero here because: 1. the delay model in the literature was developed for adults and the correct parameter values are unknown for fetuses; 2. computational cost is much higher for a delayed differential equation system for 4-hour simulations rather than a few minutes as in [24]). In addition, this transient growth due to delay does not seem to affect the general feature of our model outcome including the metabolic dynamics (reported below).

Fig. 6 displays the numerical results of FHR and MABP for variable UCOs. Complete UCO with varying frequency were motivated by experiments carried out in [13]. The FHR overshoot occurs only after a delay of more than two hours for the 1:2 UCOs, and MABP
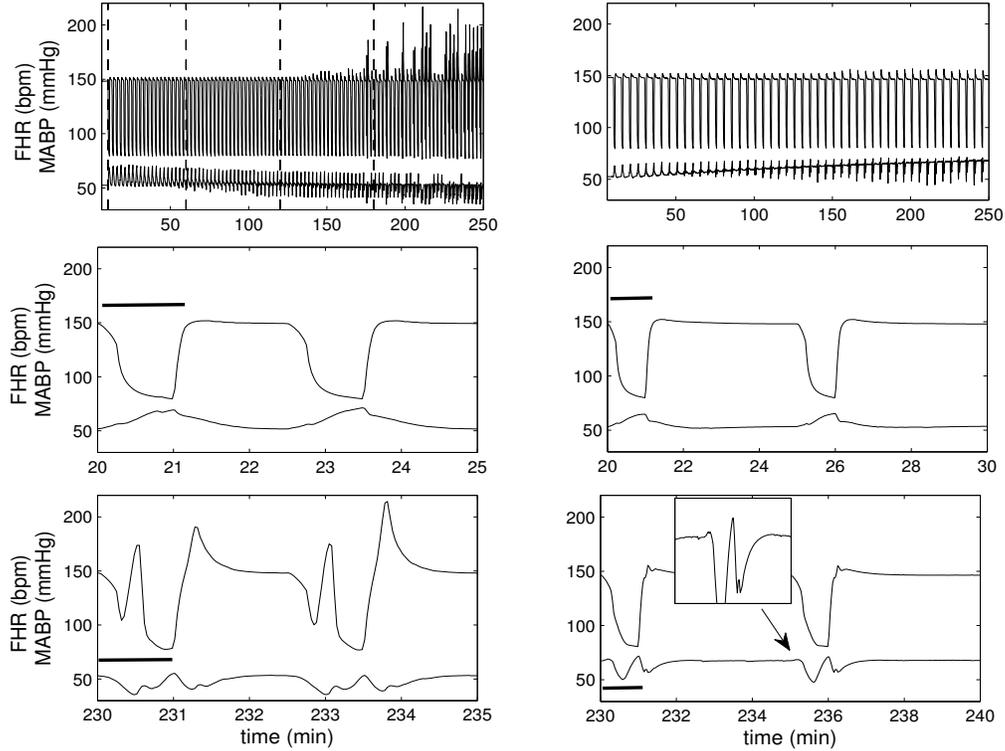
18

FIG. 5. **Numerical results of FHR and MABP for 1:2.5 and 1:5 UCO.** Numerical results for four hours of occlusions with 1:2.5 UCO (left) and 1:5 UCO (right). $G_c = 0.27$ and $G_v = -0.67$ are used in simulation with 1:5 UCO. The dashed lines in the upper left panel divide the time periods into four one-hour windows. The first dashed line marks the beginning of the occlusions. The middle row displays a zoom of 5 (left) and 10 (right) minute windows for each case at the beginning of the occlusion, and the bottom row 5 (left) and 10 (right) minute windows near the end of occlusions. The black bar indicates the occlusion duration. The inset of the right bottom panel shows that MABP rises slightly at the beginning of each occlusion, and then declines.

declines from the second hour for 1:3 UCOs. This is consistent with Fig. 5 in that relatively small frequency promotes the MABP decline and FHR overshoot. Constant frequency UCOs with varying degrees mimic experiments in [38]. Mild occlusion has little effect, but moderate occlusion decreases FHR (~ 10 mmHg) to lesser extent to complete UCOs (~ 70 mmHg). As in [38], after two hours of severe UCOs, pH drops below 7.0. Therefore, the FHR overshoot instability may be correlated with the worsening acidemia.
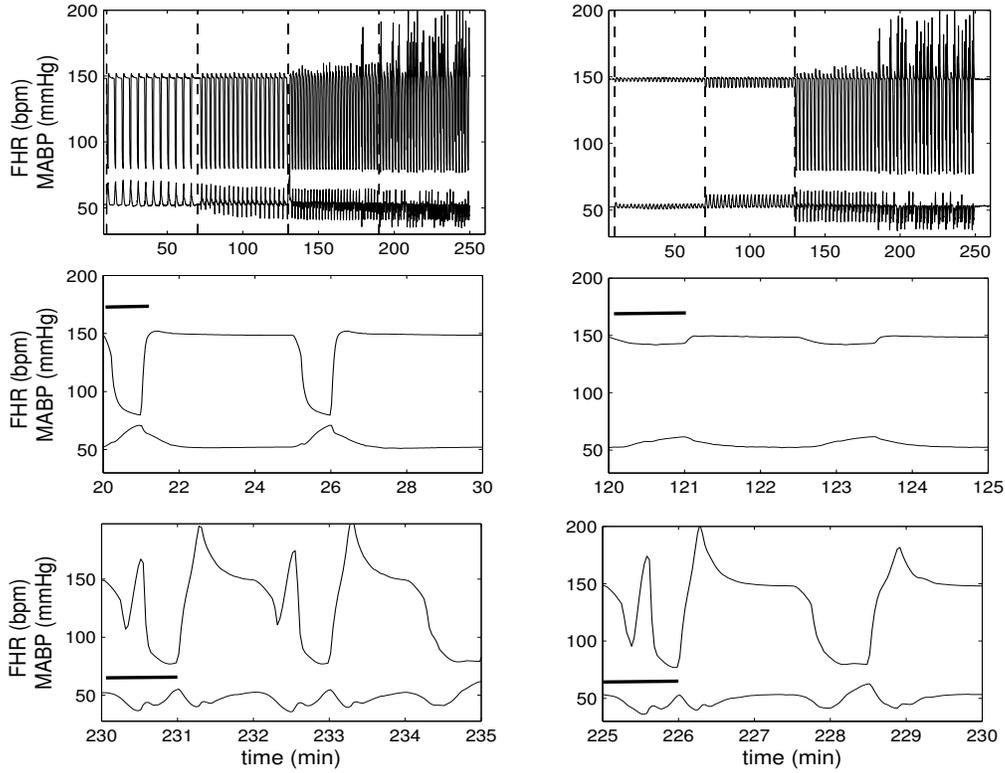
19

FIG. 6. **Numerical results of FHR and MABP for variable UCO.** Left panel: Complete UCO with varying occlusion frequency (1:5 UCO for the first, 1:3 for second, and 1:2 for the third and fourth hours). Right panel: Constant frequency UCOs with varying occlusion degree (mild occlusion during the first, moderate during the second, and severe during the third and fourth hours). Dashed lines are inserted to divide the periods into four windows, each representing one hour. The left dashed line marks the beginning of occlusions. The middle row represents 5-minute windows at the beginning of the occlusion, and the bottom row 5-minute windows near the end of occlusions. The black bar indicates the occlusion duration.

C. Metabolic dynamics

To assess the fetal acidemia, a simplified metabolic model is coupled with the cardiovascular model to evaluate pH as well as BD defined by Eq. (56) (see also [13])

$$\mathrm{BD} = -(0.02786 \mathrm{P}_{\mathrm{CO}_2} 10^{\mathrm{pH}-6.1} + 13.77 \mathrm{pH} - 124.58). \tag{56}$$
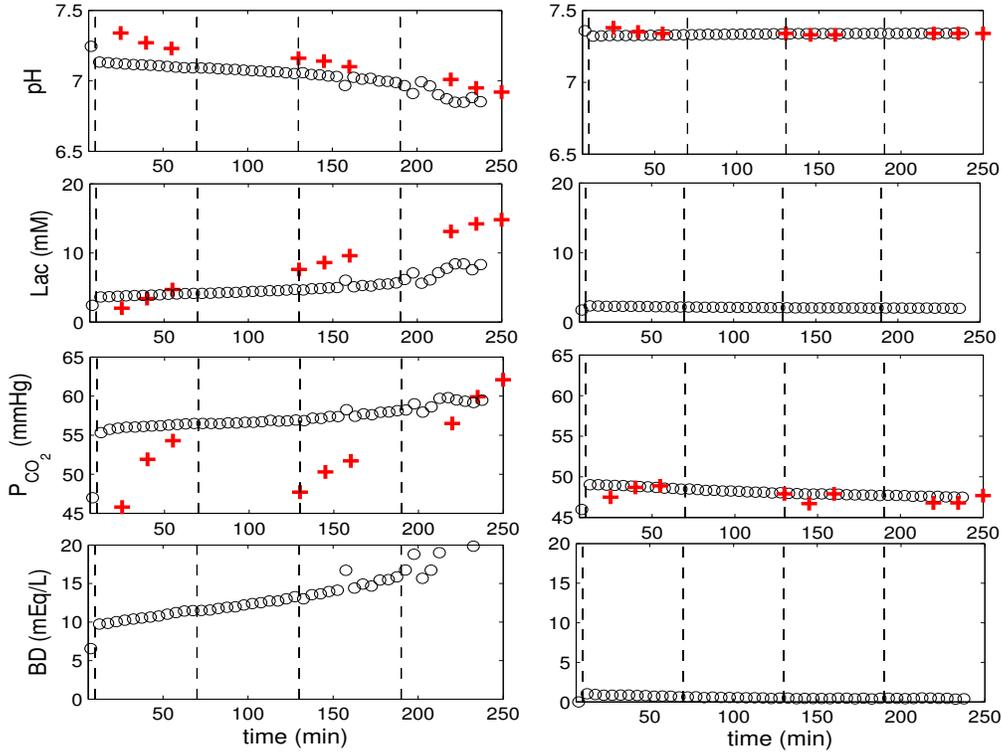
FIG. 7. **Numerical results of pH, lactate, P_{CO_2} and BD for 1:2.5 and 1:5 UCO.** Time variations of pH, lactate, P_{CO_2} in the systemic compartment and BD for 1:2.5 UCOs (left) and 1:5 UCO (right). The $'\circ'$ symbol represents the mean values over 5 minutes after occlusion begins. The $'+'$ symbol represents experimental data (table 1 in [4]).

In particular, we computed the variations of lactate, $[H^+]$ and P_{CO_2} in the systemic compartment to compare with the experimental data.

Fig. 7 shows several experimentally measurable quantities over 4-hour occlusions. Agreement is shown when comparing with the data extracted from [4]. Corresponding to the FHR overshoot instability for 1:2.5 UCO in Fig. 5, we find that pH drops below 7.00 and lactate accumulates beyond 10 mM. On the other hand, pH remains in the normal range for 1:5 UCOs, even after four hours of repeated occlusions [4, 29]. pH, lactate and P_{CO_2} remain close to baseline values. The results depicted in Fig. 8 for variable UCOs captured the experimental data trend. Relatively low-frequency UCOs and completely occluded UCOs have greater influence than those with higher frequency or partially occluded UCOs. The fetal acidosis occurs for severe UCOs, indicated by the BD values and FHR overshoot instability.
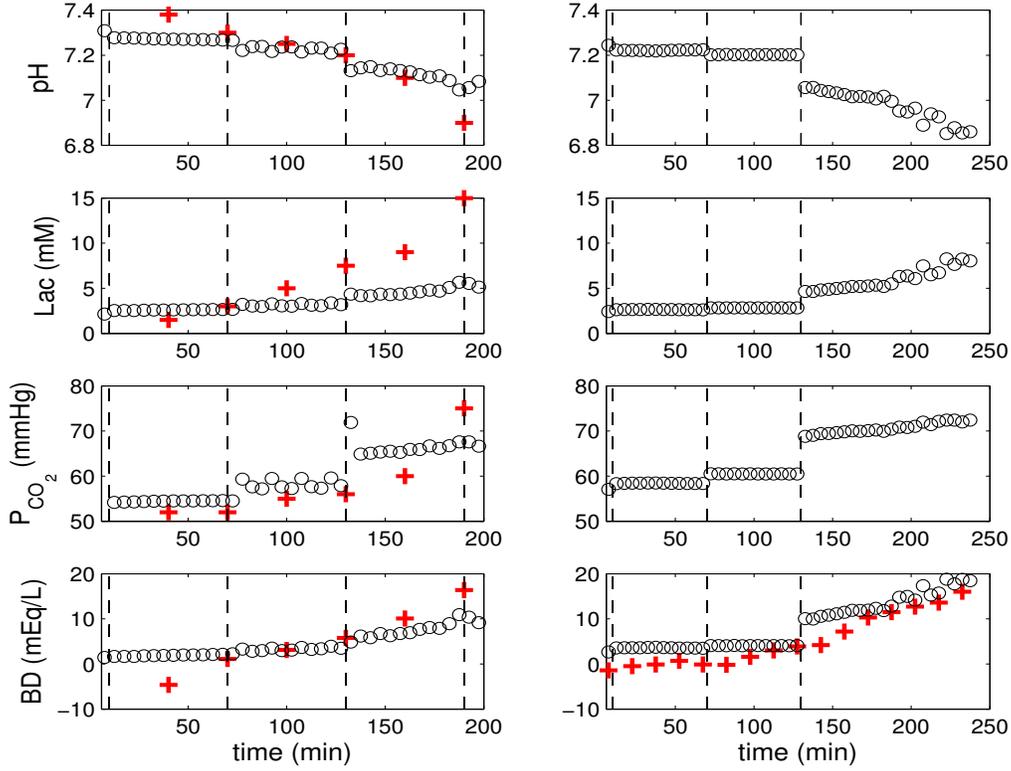
21

FIG. 8. **Numerical results of pH, lactate, P_{CO_2} and BD for variable UCOs.** Time variations of pH, lactate, P_{CO_2} and BD in the systemic compartment for complete UCO with varying frequency (left column; 1:5 UCO for the first, 1:3 for second, and 1:2 for the third and fourth hours) and UCO of varying degree with constant frequency (right column: mild occlusion during the first, moderate during the second, and severe during the third and fourth hours). In the simulations displayed by the left column, $K_7 = 35 \times 10^{-6}$ s^{-1} in Eq. 32 and $K_6 = 5$ s^{-1} are chosen to match with the experimental pH variation; $k_{CO_2} = 0.008$ in Eq. 24 is chosen to match the baseline value of $P_{CO_2} = 52.7 \pm 0.9$ mmHg in the experiments [13]. The remaining parameters are given in Tables I and II.

In an attempt to quantify the relationship of these variables, we compute the correlations between relevant quantities in Section III D.

22

D. Statistical Analysis

We begin this section by computing the contingency table for each case discussed earlier. In order to make a direct comparison with experimental data, we also present some analysis on RMSSD, an index of vagal modulation of heart rate variability.

We examined correlations between acidemia quantified by BD and lactate on one hand and FHR and MABP on the other. Due to the cyclical nature and time dependency, classical Pearson correlation is not applicable to the data considered here. Therefore, we discretize the original signal into binary time sequences with 1 indicating the occurrence of an anomaly and 0 otherwise. An anomaly is defined as an event when an observation occurs outside an estimated confidence interval of long term average. We use the mean $\tilde{\mu}$ and standard deviation $\tilde{\sigma}$ to set a threshold value, $\tilde{\mu} \pm 2\tilde{\sigma}$, in order to sort out the relevant quantities. For example, when the FHR (or BD or lactate) is larger than the upper bound threshold value $\tilde{\mu} + 2\tilde{\sigma}$, these quantities are set to 1, otherwise to zero. Similarly, when MABP is smaller than the lower bound of the threshold value $\tilde{\mu} - 2\tilde{\sigma}$, the MABP is set to 1, otherwise to zero. Contingency tables are then constructed for each pair based on the simultaneous occurrence of 1s and 0s.

For 1:2.5 UCOs, representative tables are constructed by taking the last two hours of simulation data, given in Table V. The counts in each cell record the total number of occurrence for one combination between two discretized time sequences. For example, the first cell in each table records the total numbers of normal occurrence in both time series.

To search possible correlations among FHR, MABP, lactate, and BD, two statistical tests are carried out. The first is the traditional Chi-square test and the second is on the odds ratio derived from each contingency table. Both tests reject the hypothesis that these variables are independent with very small p-values ($p < 0.0001$). Therefore, we conclude that the anomalies in these sequences are indeed correlated with each other. Same conclusion can be drawn for UCOs with varying frequencies (Table VI). These findings are consistent with our results in Sections III B and III C, as FHR overshoot, MABP declines, and lactate level increase becomes significant when large BD value appears near the end of the occlusions.

However, our results from Table VII for UCOs with variable occlusion degrees suggest that contingent table along may not be sufficient to reveal the subtle relationship among FHR and MABP and BD. Following [11, 38, 48]) via Eq. 57, we compute RMSSD based on
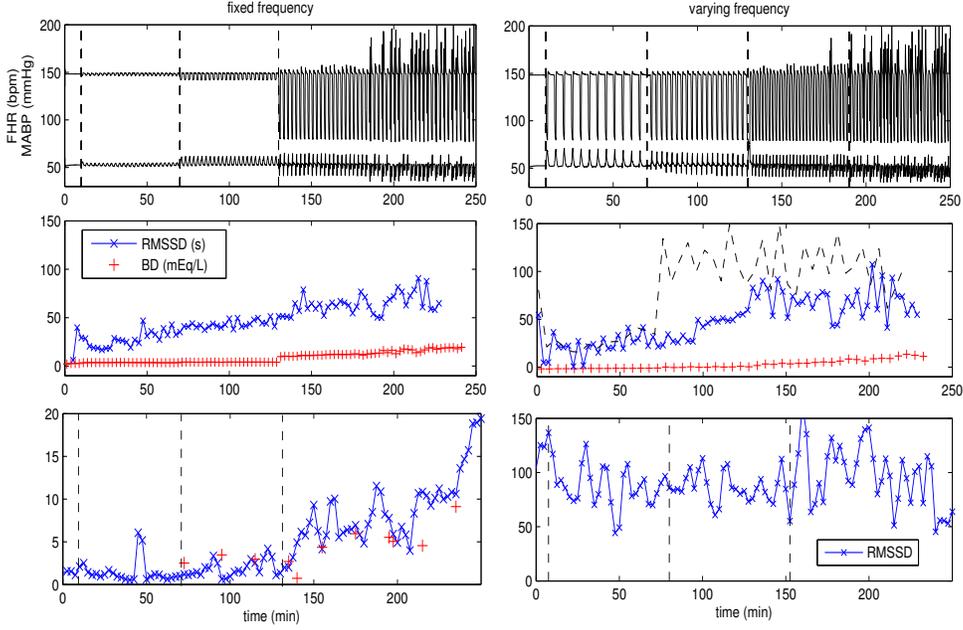
FIG. 9. **Computed RMSSD with a sampling frequency of 4 Hz and BD for UCOs with varying occlusion degrees (left) and varying frequencies (right).** Patterns of FHR (top), RMSSD and BD (middle), and the corresponding representative experimental results [46] and [47] (bottom). In the middle row, RMSSD is computed using 5-minute windows for the left column. For the right column, RMSSD is computed using both 3- (cross-symbol) and 5-minute (dashed line) windows.

our FHR output

$$RMSSD = \sqrt{\frac{1}{N-1}\left(\sum_i D_i\right)}, \tag{57}$$

where $D_i = |P_{i+1} - P_i|^2$ with P_i the period between two maximum peaks and N is the number of intervals within a certain window. For the case in the left column of Fig. 9, where the frequency is varying, the computed RMSSD qualitatively captures the trend of experimental data, which is displayed in the bottom panel (the discrepancy in magnitude is due to sampling frequency). As occlusion proceeds, RMSSD increases monotonically. The contingency tables do not exhibit significant correlation for this case. However, based on our pH and BD results, we obtain significant increase in RMSSD when acidosis occurs, compared to the baseline values.

In contrast, RMSSD is overestimated for moderate occluded UCOs as soon as occlusion

24

occurs (middle right panel using 5-minute window as indicated by the dashed line) while no obvious increase is observed afterwards. This is similar to a representative set of experimental data [47] (bottom right panel).

Interestingly, if we reduce the window size, the computed RMSSD evolves very differently. For example, RMSSD using a 3-minute window (cross-symbols, middle right panel of Fig. 9) gradually increases as UCOs proceed and acidosis develops. This suggests that, in addition to the importance of sampling frequency [48], a proper window size is also important.

IV. CONCLUDING REMARKS

We have investigated the cardiovascular and metabolic responses to UCOs in a fetal sheep circulation using a mathematical model. Our model comprises a cardiovascular circuit, a simplified metabolic model, and nervous control of blood pressure and oxygen content by baro- and chemoreceptors [18, 23, 28]. Waste accumulation in the systemic compartment, such as CO_2 and lactate, is solved simultaneously with the cardiovascular response.

Our mathematical model produces the pattern observed in animal experiments, including FHR decrease and overshoot, MABP and pH decline, and increased levels of lactate and CO_2. In particular, the development of the cardiovascular and metabolic responses in our model are the result of sufficiently long lasting repetitive occlusions. In other words, acidosis depends on the total duration of occlusion rather than on an individual event, as in [17]. In addition, the FHR decrease, FHR overshoot, and MABP response evolve accordingly to observations obtained using various experimental scenarios. In particular, our results from 1:5 and 1:2.5 UCO demonstrate the possibility that properly functioning effectors (cardiac contractility, systemic resistance, and venous compliance) are able to main the blood pressure level and avoid instabilities in FHR. Our simplified metabolic model reproduces measured changes in pH, lactate, and glucose. Although expected correlation between FHR overshoot, MABP decline, and acidosis (quantified by BD) can be obtained when the occlusion is complete, our results suggest that the correlation analysis may fail when the UCO degree varies significantly. In that case, we show RMSSD is able to qualitatively predict acidemia.

The choice of window size is important in computing RMSSD when UCO frequency varies. Uterine contractions during labour varies in frequency and degree. Therefore, the usual choice of fixed window size may affect the results obtained in [48], in addition to the

sampling frequency. A proper combination of FHR monitoring and RMSSD computation may then be used to detect acidemia.

One limitation of our model is that, as other mathematical biology models in the literature, the parameter space is large, despite our effort to keep the model simple. Although the sensitivity analysis has been carried out, physiological parameters are difficulty to estimate accurately. We plan to use statistical modeling to control the uncertainty in parameters in the future work [49]. Another limitation deals with the simplified metabolic process. A more detailed model will potentially improve predictions of impaired supply of nutrients [50]. The transport equations are used with relatively simple kinetic reaction terms involving only O_2, CO_2, pyruvate, lactate, glucose and $[H^+]$ in the systemic compartment. Nevertheless, more experimental data will be needed to properly model the kinetics and regulation.

---

[1] R. Liston, D. Sawchuck, and D. Young, J. Obstet. Gynecol. Can. **29**, 53 (2007).

[2] J. A. Low, C. Panagiotopoulos, and E. J. Derrick, Am. J. Obstet. Gynecol. **172**, 805 (1995).

[3] J. A. Westgate, L. Bennet, and A. J. Gunn, J. Obstet. Gynecol **106**, 664 (1999).

[4] L. Bennet, J. A. Westgate, Y.-C. Liu, G. Wassink, and A. J. Gunn, J. Appl. Physiol. **99**, 1477 (2005).

[5] E. Mallard, C. E. Williams, B. M. Johnston, M. I. Gunning, and e. a. S. Davis, Pediatr Res. **37**, 707 (1995).

[6] B.J.Koos, A. Chau, and D. Qgunyemi, J. Physio. **488**, 761 (1995).

[7] J. M. Bishai, A. B. Blood, C. J. Hunter, L. D. Longo, and G. G. Power, J. Physiol. **456**, 869 (2003).

[8] C. Hunteri, A. Blood, ..., and G. G. Power, J. Physiol. **552**, 241 (2003).

[9] J. A. Westgate, B. Wibbens, L. Bennet, G. Wassink, J. T. Parer, and A. J. Gunn, Am. J. Obstet. Gynecol **197**, 236.e1 (2007).

[10] A. S. Thakor and D. A. Giussani, Am. J. Physiol. Regul. Integr. Comp. Physiol. **296**, R90 (2008).

[11] M. Frasch, T. Muller, D. Hoyer, C. Weiss, H. Schubert, and M. Schwab, Am. J. Physiol. Regul. Integr. Comp. Physiol. **296**, R702 (2009).

[12] M. Frasch, B. Frank, M. Last, and T. Muller, Front Physiol. **3**, 378 (2012).

[13] M. Frasch, R. Z. Mansano, R. Gagnon, B. S. Richardson, and M. G. Ross, AJOG **200**, 200.e1 (2009).

[14] E. B. Yan, A. A. Baburamant, A. M. Walker, and D. W. Walker, Am. J. Physiol. Regul. Integr. Comp. Physiol. **297**, R60 (2009).

[15] A. Jensen, Y. Garnier, and R. Berger, Eu. J. Obstet. Gynecol. Reprod. Biol. **84**, 155 (1999).

[16] S. K. Agrawal, F. Doucette, R. Gratton, B. Richardson, and R. Gagnon, Obstet. Gynecol **102**, 731 (2003).

[17] H. H. de Haan, A. J. Gunn, and P. D. Gluckman, Am. J. Obstet. Gynecol **176**, 8 (1997).

[18] M. Ursino, Am. J. Physiol. **275**, H1733 (1998).

[19] M. Ursino and E. Magosso, Am. J. Physiol. Heart Circ. Physiol. **279**, H149 (2000).

[20] M. Ursino and E. Magosso, Am. J. Physiol. Heart Circ. Physiol. **284**, H1479 (2003).

[21] F. Liang and H. Liu, J. Physio. Sci. **56**, 45 (2006).

[22] F. Liang, S. Takagi, and R. Himeno, Med. Bio. Eng. Comput. **47**, 743 (2009).

[23] M. B. van der Hout-van der Jagt, S. G. Oei, and P. H. M. Bovendeerd, Early Human Development **89**, 7 (2013).

[24] M. S. Olufsen, H. T. Tran, and J. T. Ottesen, Cardiovascular Engineering: An International Journal **4**, 47 (2004).

[25] M. S. Olufsen, J. T. Ottesen, H. T. Tran, L. M. Ellwein, L. A. Lipsitz, and V. Novak, J. Appl. Physiol. **99**, 1523 (2005).

[26] L. M. Ellwein, H. T. Tran, C. Zapata, V. Novak, and M. S. Olufsen, Cardiovasc. Eng. **8**, 94 (2008).

[27] Y. Shi, L. Patricia, and H. Rodney, Biomed Eng Onlin **10**, 1 (2011).

[28] M. B. van der Hout-van der Jagt, S. G. Oei, and P. H. M. Bovendeerd, Med. Eng. Phys. **34**, 579 (2012).

[29] J. A. Westgate, L. Bennet, H. de Haan, and A. J. Gunn, Obstet. Gynecol **97**, 454 (2001).

[30] P. M. S. Couto, W. L. van Meurs, J. Bernardes, J. P. M. de Sa, and J. A. Goodwin, Control Eng Prac **10**, 59 (2002).

[31] M. C. Khoo, A. Gottschalk, and A. I. Pack, J. Appl. Physiol. **70**, 2014 (1991).

[32] M. C. Khoo, R. E. Kronauer, K. P. Strohl, and A. S. Slutsky, J. Appl. Physiol: Respirat. Environ. Exercise Physiol. **53**, 644 (1982).

[33] M. Ross, M. Jessie, K. Amaya, B. Matushewski, L. D. Durosier, M. G. Martin, and B. S. Richardson, Am. J. Obstet Gynecol. **208:285**, e1 (2013).

[34] M. E. Cabrera, G. M. Saidel, and S. C. Kalhan, Ann. Biomed. Eng. **26**, 1 (1998).

[35] C. D'Angelo and Y. Papelier, ESAIM: Proceedings **14**, 72 (2005).

[36] P. Orlowski, M. Chappell, C. S. Park, V. Grau, and S. Payne, Interface focus **1**, 408 (2011).

[37] E. Magosso and M. Ursino, Am. J. Physiol. Heart Circ. Physiol. **281**, H2036 (2001).

[38] M. Frasch, T. Muller, D. Hoyer, C. Weiss, H. Schubert, and M. Schwab, Reprod. Sci. **16**, 509 (2009).

[39] T. Kubota, J. Alexander, R. Itaya, K. Todaka, M. Sugimachi, K. Sunagawa, and Y. Nose, Circ. Res. **70**, 1044 (1992).

[40] T. Kubota, H. Chishaki, T. Yoshida, K. Sunagawa, A. Takeshita, and Y. Nose, Am. J. Physiol. **263**, H307 (1992).

[41] M. N. Levy and H. Zieske, J. Appl. Physiol. **27**, 465 (1969).

[42] D.-I. Marc Breit, *Sensitivity analysis of biological pathways*, Master's thesis, University for Health Sciences, Medical Informatics and Technology, Germany (2004).

[43] M. Frasch, A. Keen, R. Gagnon, M. Ross, and B. Richardson, PLoS One **6**, e22100 (2011).

[44] E. J. Quilligan, A. Vasicka, R. Aznar, P. J. Lipsitz, T. Moore, and B. M.Bloor, Am. J. Obstet Gynecol. **79**, 1048 (1960).

[45] R. Gui, C. Sch uthe, and S. Bernhard, ZIB-Report(2015).

[46] M. G. Frasch, N. Gold, C. Herry, B. S. Richardson, A. J. E. Seely, and X. Wang, Bioinformatics **in preparation** (2015).

[47] X. Wang, L. D. Durosier, M. G. Ross, B. S. Richardson, and M. G. Frasch, PLoS One **9**, PMC4182309 (2014).

[48] L. D. Durosier, G. Green, I. Batkin, A. J. Seely, M. G. Ross, B. S. Richardson, and M. G. Frasch, Front. Pediatr **2**, PMC4017161 (2014).

[49] J. O. Ramsay, G. Hooker, D. Campbell, and J. Cao, J. R. Statist. Soc. B **69**, 741 (2007).

[50] M. Cloutier, F. B. Bolger, J. P. Lowry, and P. Wellstead, J. Comput. Neurosci. **3**, 391 (2009).

TABLE I. Parameter values.

parameter (cardiovascular model)	value	parameter	value
c_f (mmHg/cm^3)	0.9	c_m (mmHg/cm^3)	1.5
d_m (mmHg)	1.1264	d_f	5
ψ (1/s)	0.05	H_m (1/s)	0.9
C_a (ml/mmHg)	0.8	C_v (mmHg s/ml^3)	3.5
C_{um} (ml/mmHg)	1.1	C_c (mmHg s/ml^3)	0.057
R_a (mmHg s/ml^3)	0.045	R_v (mmHg s/ml^3)	0.27
R_{mc0} (mmHg s/ml^3)	1.5	R_{umv} (mmHg s/ml^3)	0.015
R_{cv} (mmHg s/ml^3)	0.015	R_{cmc0} (mmHg s/ml^3)	10.485
parameter (regulation model)	value	parameter	value
$R_{mc,min}$ (mmHg s/ml^3)	0	$R_{mc,max}$	11.25
T_0 (s)	0.406	T_{v0} (s)	0.373
T_{s0} (s)	-0.177	$P_{O_{2a,n}}$ (mmHg)	7.5
f_{evmin} (1/s)	3.2	f_{evmax} (1/s)	6.3
f_{esmin}	2.66	f_{esmax}	60
f_{es0}	16.11	f_{esinf}	2.1
f_{vn} (1/s)	10	τ_{gs} (1/s)	0.05
$f_{shn,0}$ (1/s)	8	τ_{gv} (1/s)	0.04
k_{es}	0.0675	k_{ev} (mmHg^{-1})	7.06
W_{cv}	0.2	W_{bv}	1
$G_{T,s}$ (s^2)	-0.13	$G_{T,v}$ (s^2)	0.04
$G'_{T,s}$ (s^2)	0.046	δG_T (s^2)	0.1235
$\tau_{T,s}$ (s)	6	τ_{isc} (s)	30
f_{ac} (mmHg)	11	$f_{ab,n}$ (mmHg)	25
G_c	0.27	G_v	-0.17

TABLE II. Parameter values.

parameter (metabolic model)	value	parameter	value
$[O_2]_{a,0}$ (ml^3 O$_2$/ml^3 blood)	0.04	k_a	0.005
K_f (ml^3 blood)	9.33	$[O_2]_{th}$ (ml^3 O$_2$/ml^3 blood)	0.068
K_{CO_2} (ml^3 O$_2$/ml^3 blood/mmHg)	0.244	k_{CO_2} (ml^3 O$_2$/ml^3 blood)	0.007
D_{CO_2} (ml CO$_2$/s/mmHg)	0.1	k_{um} (ml CO$_2$/s)	0.2
GL$_a$ (mM)	1	LA$_a$ (mM)	0.8
Py$_a$ (mM)	0.12	$[H^+]_a$ (nM)	40
K_1 (mM/s)	100	K_2 (1/s)	40
K_3 (1/s)	0.4	K_4 (1/s)	4
K_5 (1/s)	0.5	K_6 (1/s)	10
K_7 (10^{-6}1/s)	55	K_8 (nmol/s)	10
K_9 (nM/s)	15	K_{10} (10^6 1/s)	0.2

TABLE III. Clinically relevant quantities.

Baseline case		
physical quantity	reference/target value	model output
FHR (bpm)	135 [28], 163±5 [43]	148
mean fetal arterial $\bar{p}_a$ (mmHg)	55± 5 [4], 46±2 [8]	52.5
umbilical P$_{O_2}$ (mmHg)	18 [28]	17.6
cerebral P$_{O_2}$ (mmHg)	10±1 [7]	12.3
systemic P$_{CO_2}$ (mmHg)	45.5±2 [4] 52.7± 0.9 [38, 43]	47.5
intervillous space P$_{O_2}$ (mmHg)	23.3 [28, 44]	23.2
systemic lactate (mM)	1.6±0.2 [38]	2.1
systemic pH	7.36± 0.1 [38], 7.4±0.01 [4]	7.25

Parameter	Role	Effect
$G_{T,v}$	vagal gain	Increase the contribution to heart period by vagal activity
W_{bv}	weight factor in f_v in (40)	Increase the contribution due to baroreflex in vagal firing rate
f_{evmax}	maximum in sigmoid curve due to baroreflex	Increase f_v in (40)
$W_{b,sh}$	factor in front of f_{ab} in (40)	Decrease f_{sh}
$f_{es,min}$	threshold in (41)	Increase the inactive range f_s
P_n	threshold to trigger baroreceptor in (45)	Reduce the time to obtain the FHR overshoot
k_{es}	factor in the exponent of (43)	Increase the steepness of sigmoid curve in (43)
W_{cv}	weight factor in front of f_{ac} in (40)	Increase f_v
f_{es0}	factor in (43)	Increase $f_{sh/sp}$
$P_{O_2,0}$	threshold to trigger chemoreceptor in (42)	Promote the chemoreflex

TABLE IV. Descriptions of the Top 10 most sensitive parameters in model.

TABLE V. **Contingency tables for 1:2.5 UCO.** X represents for the binary series for FHR, MABP and lactate from left to right respectively, while Y represents for BD.

	$Y = 0$	$Y = 1$		$Y = 0$	$Y = 1$		$Y = 0$	$Y = 1$
$X = 0$	3303	266	$X = 0$	3167	251	$X = 0$	3204	31
$X = 1$	4	27	$X = 1$	140	42	$X = 1$	103	262

TABLE VI. **Contingency tables for UCO with various frequencies.** X represents for the binary series for FHR, MABP and lactate from left to right respectively, while Y represents for BD.

	$Y = 0$	$Y = 1$		$Y = 0$	$Y = 1$		$Y = 0$	$Y = 1$
$X = 0$	3250	324	$X = 0$	3137	304	$X = 0$	3151	74
$X = 1$	4	22	$X = 1$	117	42	$X = 1$	103	272

TABLE VII. **Contingency tables for UCO with various degrees.** X represents for the binary series for FHR, MABP and lactate from left to right respectively, while Y represents for BD.

	$Y = 0$	$Y = 1$		$Y = 0$	$Y = 1$		$Y = 0$	$Y = 1$
$X = 0$	3220	376	$X = 0$	3135	372	$X = 0$	3118	92
$X = 1$	2	2	$X = 1$	87	6	$X = 1$	104	286